


Article

Natural Characteristics Analysis of a Dual-Rotor System with Nonparametric Uncertainty

Hangfei Wu ^{1,2}, Baoguo Liu ^{1,2,*}, Yanxu Liu ^{1,2} and Wei Feng ^{1,2} ¹ School of Mechanical and Electrical Engineering, Henan University of Technology, Zhengzhou 450001, China² Henan Key Laboratory of Super Hard Abrasives Grinding Equipment, Zhengzhou 450001, China

* Correspondence: bgliu1978@sina.com

Abstract: In order to evaluate the impacts of parameter uncertainty and nonparametric uncertainty on the natural characteristics of a dual-rotor system, a nonparametric probabilistic method based on random matrix theory is proposed. In this paper, a nonparametric Riccati whole transfer model is derived based on the maximum entropy principle and the random matrix theory. It is used to model a dual-rotor system with nonparametric uncertainty, as well as to calculate the natural characteristics of the system. Furthermore, the impacts of parameter uncertainty and nonparametric uncertainty on the natural characteristics at the intermediate support element and at the disk-shaft element are discussed using numerical simulations, and the results are compared with related references. The results show that at the same level of uncertainties, the effect of nonparametric uncertainty is often more significant than that of parameter uncertainty. The effects of uncertainties also increase with the level of uncertainties. The results of this paper provide a theoretical basis for the design of uncertain dual-rotor and multi-rotor systems.

Keywords: nonparametric uncertainty; parameter uncertainty; critical speed; vibration mode; maximum entropy random model



Citation: Wu, H.; Liu, B.; Liu, Y.; Feng, W. Natural Characteristics Analysis of a Dual-Rotor System with Nonparametric Uncertainty. *Appl. Sci.* **2022**, *12*, 12573. <https://doi.org/10.3390/app122412573>

Academic Editor: Keun Ryu

Received: 28 October 2022

Accepted: 4 December 2022

Published: 8 December 2022

Publisher's Note: MDPI stays neutral with regard to jurisdictional claims in published maps and institutional affiliations.



Copyright: © 2022 by the authors. Licensee MDPI, Basel, Switzerland. This article is an open access article distributed under the terms and conditions of the Creative Commons Attribution (CC BY) license (<https://creativecommons.org/licenses/by/4.0/>).

1. Introduction

Rotor systems are widely used in aero-engines, gear transmissions, large steam wheels, and other machines [1]. In some cases, the operating conditions of these systems are pretty serious. Moreover, they will cause significant damage to economic and personal safety if an accident occurs. Therefore, it is essential to carry out a rigorous dynamic characteristics analysis for rotor systems in the design process [2,3]. So far, many studies on rotordynamics modeling methods have been published. However, there are a lot of uncertainties in the whole life cycle of a device from design, to manufacturing, to operation, to maintenance, which have great impacts on the operation of the device. These uncertainties can then be split into two classes, i.e., aleatoric uncertainty and epistemic uncertainty [4]. The former is mainly caused by changes in operating conditions and errors and is always used to consider the uncertainty of the geometric parameters and physical parameters of the system [5], also known as parameter uncertainty, which has already received great attention and sufficient research in recent years; the latter is induced from the difficulty of accurately modeling the dynamic characteristics of a system [6,7], known as nonparametric uncertainty, which is mainly introduced by modeling the actual systems abstractly and has become a hot topic in the field of stochastic rotor dynamics.

It is the stochastic parametric method that is used to deal with the parametric uncertain problem. In essence, it allows some random variables to be used to describe the uncertain parameters in the dynamic model, and then, one can combine it with the finite element method (FEM) and the Monte Carlo simulation (MCS) to study uncertainties. Nevertheless, it cannot take nonparametric uncertainty induced by model errors and calculation errors into account [8]. For instance, Fu et al. [9,10] proposed a noninvasive metamodeling method

to quantify the parameter uncertainty of a dual-rotor system and calculated the steady-state nonlinear dynamic response of the system under interval uncertainty. Wang et al. [11] proposed the non-probabilistic Chebyshev convex method (CCM) and calculated critical speeds and dynamic responses. The results indicate that the response of the rotor system is no longer deterministic, but rather, it varies in an interval. For nonparametric uncertainty, a nonparametric probabilistic method based on random matrix theory (RMT) has been proposed and widely used, so it will be studied in this paper. Soize [12–15], who introduced RMT into structural dynamics and developed a large number of fundamental theories, conducted pioneering research in the study of the stochastic dynamics of nonparametric uncertainty systems. Murthy et al. [16] introduced the maximum entropy principle (MEP) into the nonparametric modeling method and obtained a nonparametric transfer model of a single rotor system, further analyzing the action of uncertainties on the eigenvalues of the system. Gan et al. [17,18] not only constructed a nonparametric model of the classic Jeffcott rotor but also studied the effects of nonparametric uncertainty on the critical speeds and unbalanced responses of the rotor with different disk-offsets via numerical simulation. Huang et al. [19] used a nonparametric method to model a high-speed motorized spindle with uncertainty and discussed vibration responses. However, the effects of the two uncertainties were not distinguished. Liu et al. [20] proposed a nonparametric model of a dual-rotor system and investigated the effects of two uncertainties on the critical speeds of the system but did not discuss the impacts on the vibration modes. The above studies show that it is feasible to use the nonparametric modeling method to analyze rotor systems with uncertainty. Nevertheless, most of the investigations focus on the critical speeds and dynamic responses of a single-rotor system. Furthermore, both types of uncertainties have an effect on vibration modes, but the current research has only considered parameter uncertainty. In this paper, the impacts of nonparametric uncertainty on the vibration modes of dual-rotor and multi-rotor systems are discussed, which makes up for the shortcomings of the current research.

In this paper, a nonparametric Riccati whole transfer model is proposed for modeling uncertain dual-rotor systems. The primary purposes are calculating the natural characteristics of the uncertain dual-rotor system, such as critical speeds and vibration modes. Furthermore, the changes in the natural characteristics with uncertainties and the effects of two types of uncertainties on the natural characteristics under the same level of uncertainty are analyzed. First, the deterministic model and the nonparametric model of a dual-rotor system are described in Sections 2 and 3, respectively. Then, the impacts of two types of uncertainties on natural characteristics are studied using multiple numerical simulations in Section 4. Finally, in Section 5, the conclusions will be drawn.

2. Deterministic Model of a Dual-Rotor System

2.1. Calculation Model of a Dual-Rotor System

This paper cites the calculation model from Reference [21], and a structure diagram of a dual-rotor system with a single intermediary support is shown in Figure 1. The system is divided into 10 nodes according to the concentrated mass rigid disk, massless elastic shaft segment, and support. It consists of two rotors: rotor *I* is an inner rotor, and rotor *II* is an outer rotor. Rotor *I* is connected to the base by the first and sixth nodes, while the left end of rotor *II* is connected to the base by the seventh node, and the right end is connected to rotor *I* by the tenth node. The detailed parameters are provided in Table 1.

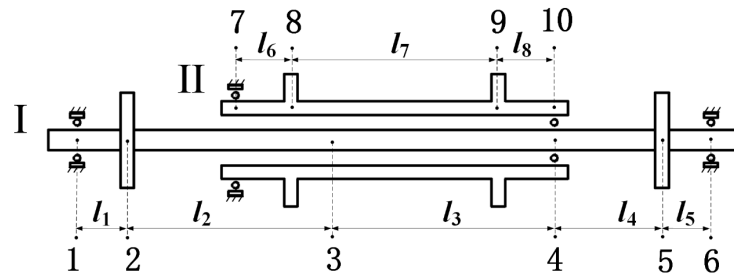


Figure 1. Structure diagram of the dual-rotor system.

Table 1. The parameters of the dual-rotor system.

Rotor	Speed $\omega/(\text{rad}\cdot\text{s}^{-1})$	Stiffness of Rotor $J/(\text{m}^4)$	Station	Mass m/kg	Moment of Inertia $I_p/(\text{kg}\cdot\text{m}^2)$	Stiffness of Element $k \times 10^{-7}$	Length $l/(\text{m})$
I	1047.2	2.6467×10^{-9}	1	0.05770	0	0.6269	0.0762
			2	10.7023	0.0859		0.1778
			3	0.24990	0		0.1524
			4	0.15380	0	0.8756	0.0508
			5	7.08690	0.0678		0.0508
			6	0.03850	0	1.7513	
II	1570.8	2.1935×10^{-3}	7	0.04699	0	1.7513	0.0508
			8	7.20200	0.0429		0.1524
			9	3.69200	0.0271		0.0508
			10	0.04699	0	0.8756	

From Figure 1, the number of nodes in rotor I and II are unequal, which is counter to constructing a whole transfer matrix. Nevertheless, virtual elements with zero mass and zero length are added at both end sections of the dual-rotor system, and the number of elements is reset [22]. The two rotors are also elastomers; the 2nd, 3rd, 5th, 6th, 7th, 8th, 10th, and 11th elements are elastomers, and the 4th and 9th elements are rigid bodies. Therefore, the elastic deformation will also have an impact on the dynamic characteristics of the system, which must be taken into account [23–25]. This problem will be studied in the following section. The dual-rotor system, after resetting, is shown in Figure 2. All the derivation processes described later in this paper are based on it.

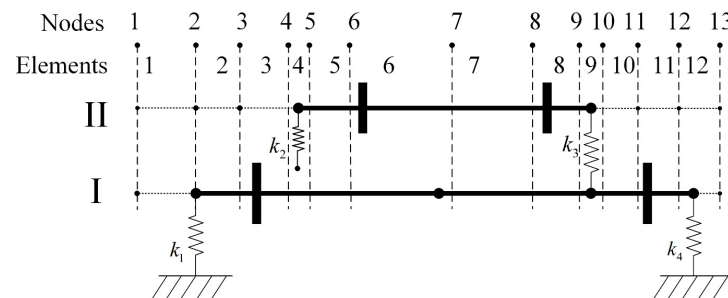


Figure 2. Element division of the dual-rotor system.

The state vector of the i th node of rotors I and II can be written as $\mathbf{Z}_i^I = [M^I, Q^I, x^I, \theta^I]^T$ and $\mathbf{Z}_i^{II} = [M^{II}, Q^{II}, x^{II}, \theta^{II}]^T$, where the parameters M , Q , x , and θ are the bending moment, shear force, displacement, and rotation angle, respectively. To facilitate the construction of the transfer model in the overall elements, \mathbf{Z}_i^I and \mathbf{Z}_i^{II} are combined in the state vector, \mathbf{Z}_i .

$$\mathbf{Z}_i = \begin{bmatrix} \mathbf{Z}_i^I \\ \mathbf{Z}_i^{II} \end{bmatrix} \quad (1)$$

Since this system is a complex rotor system composed of two rotors, the traditional transfer matrix method for a single-rotor system is no longer applicable. Therefore, the whole transfer matrix method is introduced to build the whole transfer model of this dual-rotor system. In the deterministic modeling of this system, the coupling actions at the coupling element need to be considered. In contrast, such effects need not be considered in the uncoupled element. The mean transfer model is usually used to describe a deterministic dynamic system. From transfer matrix theory [22], it is known that the state vectors of adjacent nodes agree with the following deterministic transfer model.

$$\mathbf{Z}_{i+1} = \mathbf{T}_i \mathbf{Z}_i = \begin{cases} \mathbf{C}_i \mathbf{U}_i \mathbf{Z}_i & \text{coupling element} \\ \mathbf{U}_i \mathbf{Z}_i & \text{uncoupled element} \end{cases} \quad (2)$$

where \mathbf{T}_i is the whole mean transfer matrix of each element, and \mathbf{U}_i is that of the uncoupled element. At the same time, \mathbf{C}_i is the coupling matrix.

2.2. The Riccati Whole Mean Transfer Model of the Uncoupled Element

Reference [26] points out that a maximum entropy random matrix can be constructed by combining RMT and MEP. Nevertheless, the whole mean transfer matrix has to be known in this process. As a consequence, this Sections 2.2 and 2.3 will focus on how to construct the Riccati whole mean transfer matrix of any element. Meanwhile, the construction method of the maximum entropy random matrix will be provided in detail in Sections 3.1 and 3.2.

There are no intermediary supports in the uncoupled elements. Consequently, the transfer matrices need not consider the action of the coupling matrix. That is, the coupling term in the whole mean transfer matrices is zero. Therefore, the \mathbf{U}_i can be expressed as

$$\mathbf{U}_i = \begin{bmatrix} \mathbf{U}^I & \mathbf{0} \\ \mathbf{0} & \mathbf{U}^{II} \end{bmatrix}_i \quad (3)$$

where \mathbf{U}^j_i can be written as

$$\mathbf{U}^j_i = \begin{bmatrix} 1 & l^j & (m^j \omega^2 - k_s^j) l^j & (J_p^j - J_d^j \frac{\Omega^j}{\omega}) \omega^2 \\ 0 & 1 & m^j \omega^2 - k_s^j & 0 \\ \frac{(l^j)^2}{2(EI)^j} & \frac{(l^j)^3(1-\Gamma)}{6(EI)^j} & 1 + \frac{(m^j \omega^2 - k_s^j)(l^j)^3(1-\Gamma)}{6(EI)^j} & l^j + \frac{(J_p^j - J_d^j \frac{\Omega^j}{\omega})(l^j)^2 \omega^2}{2(EI)^j} \\ \frac{l^j}{(EI)^j} & \frac{(l^j)^2}{2(EI)^j} & \frac{(m^j \omega^2 - k_s^j)(l^j)^2}{2(EI)^j} & 1 + \frac{(J_p^j - J_d^j \frac{\Omega^j}{\omega}) l^j \omega^2}{(EI)^j} \end{bmatrix}_i \quad (4)$$

where $m^j_i, l^j_i, E^j_i, I^j_i,$ and Ω^j_i represent the concentrated mass, shaft segment length, elastic modulus, section moment of inertia, and rotation angular velocity of the j th rotor at the i th element, respectively; $J_p^j_i$ and $J_d^j_i$ are the polar moment of inertia and the diametric moment of inertia at the rigid thin disk, respectively; $k_s^j_i$ is the total stiffness of the connection between the shaft segment and base; ω is the angular velocity of precession; $\Gamma = 6 EJ/(ktGA l^2)$ is the shear influence coefficient; G and A are the material shear modulus and cross-section area; and k_t is the cross-section coefficient (0.886 for solid shafts and 2/3 for thin-walled hollow shafts).

From Equations (3) and (4), the whole mean transfer matrices of the uncoupled elements can be derived. Yet, with a large number of nodes in the system, a computer value overflow will occur; furthermore, it may appear that a large number subtracts another large number in calculating the vibration modes, which will decrease the calculation accuracy and result in the vibration mode distortion [27]. To avoid the above matters, the Riccati

whole mean transfer matrices, S_i , of the uncoupled elements are constructed by using the method in Reference [21], and the calculation formula is as follows:

$$S_{i+1} = \left(\begin{bmatrix} \underline{U}_{11}^I & \mathbf{0} \\ \mathbf{0} & \underline{U}_{11}^{II} \end{bmatrix}_i S_i + \begin{bmatrix} \underline{U}_{12}^I & \mathbf{0} \\ \mathbf{0} & \underline{U}_{12}^{II} \end{bmatrix}_i \right) \cdot \left(\begin{bmatrix} \underline{U}_{21}^I & \mathbf{0} \\ \mathbf{0} & \underline{U}_{21}^{II} \end{bmatrix}_i S_i + \begin{bmatrix} \underline{U}_{22}^I & \mathbf{0} \\ \mathbf{0} & \underline{U}_{22}^{II} \end{bmatrix}_i \right)^{-1} \tag{5}$$

where $\underline{U}_{11,i}^j, \underline{U}_{12,i}^j, \underline{U}_{21,i}^j, \underline{U}_{22,i}^j$ represent the two-order block matrix obtained by dividing the whole mean transfer matrix, \underline{U}_i , and \underline{S}_1 is a four-order zero matrix.

2.3. The Riccati Whole Mean Transfer Model of the Coupling Element

The transfer relationship between state vectors Z_{i+1} and Z_i on the left and right nodes at the coupling elements is provided in Equation (2), which can be expressed as

$$Z_{i+1} = \underline{U}_{C,i} Z_i \tag{6}$$

$$\underline{U}_{C,i} = C_i \underline{U}_i \tag{7}$$

where $\underline{U}_{C,i}$ represents the whole mean transfer matrix at the coupling elements, and the coupling matrix C_i can be expressed as [21]

$$C_i = \begin{bmatrix} 1 & 0 & 0 & 0 & 0 & 0 & 0 & 0 \\ 0 & 1 & -k_c & 0 & 0 & 0 & k_c & 0 \\ 0 & 0 & 1 & 0 & 0 & 0 & 0 & 0 \\ 0 & 0 & 0 & 1 & 0 & 0 & 0 & 0 \\ 0 & 0 & 0 & 0 & 1 & 0 & 0 & 0 \\ 0 & 0 & k_c & 0 & 0 & 1 & -k_c & 0 \\ 0 & 0 & 0 & 0 & 0 & 0 & 1 & 0 \\ 0 & 0 & 0 & 0 & 0 & 0 & 0 & 1 \end{bmatrix}_i \tag{8}$$

where k_c represents the linear stiffness of the intermediate supports.

The whole mean transfer matrix at the coupling element is transformed into the Riccati whole mean transfer matrix, $\underline{S}_{C,i}$, and then, the process can be calculated as follows:

$$\underline{S}_{C,i}^R = \underline{S}_{C,i}^L + \underline{R}_i \tag{9}$$

where the superscripts R and L represent the right and left end sections at the coupling element, and \underline{R}_i is the stiffness matrix at the intermediary support element, which can be expressed as

$$\underline{R}_i = \begin{bmatrix} 0 & 0 & 0 & 0 \\ -k_c & 0 & k_c & 0 \\ 0 & 0 & 0 & 0 \\ k_c & 0 & -k_c & 0 \end{bmatrix}_i \tag{10}$$

3. Nonparametric Model and Eigenvalue Solution

3.1. Probabilistic and Statistical Characteristics of Maximum Entropy Stochastic Models

The RMT was first proposed by Wishart [28] in statistics, and then it caught wide attention in the field of nuclear physics and other fields. In recent years, Soize introduced it to structural dynamics and induced the nonparametric probabilistic model to describe the dynamic characteristics of systems with nonparametric uncertainty. After continuous development, the nonparametric modeling method has gradually become the most widely used method to solve uncertainty problems in structural dynamics, vibration noise, rotordynamics, and so on.

In RMT, entropy represents the uncertainty degree of a random matrix under known constraints [16]. The MEP indicates that the one with the most entropy is closest to the actual systems among all probability density functions that satisfy the constraints.

Reference [26] shows that the key to constructing nonparametric probabilistic models is to propose the maximum entropy random matrix corresponding to the mean matrix. The obtained maximum entropy random matrix is a positive definite matrix; nevertheless, the transfer matrix in the real uncertain dual-rotor system is not always a positive definite matrix, so it is essential to transform the random matrix, B , into a positive definite form. The singular values decomposition (SVD) of B is performed as follows:

$$B = M \Sigma V^T \tag{11}$$

where M and V are both unitary matrices, and $V^T V = I$ is an identity matrix. According to this property, we can obtain the following expression:

$$B = DA \tag{12}$$

$$\begin{cases} D = MV^T \\ A = V \Sigma V^T \end{cases} \tag{13}$$

where D is a unitary matrix, and A is a symmetric positive definite random matrix.

From Equations (11)–(13), it can be known that when constructing the random matrix, B , it can be transformed into the symmetric positive definite random matrix, A , through matrix transformation. Assuming p_A is the probability density function of A , it must satisfy the three constraints of a stochastic system.

$$\int p_A(A) \tilde{d}A = 1 \tag{14}$$

$$\int A p_A \tilde{d}A = \underline{A} \tag{15}$$

$$\int \ln(\det(A)) p_A(A) \tilde{d}A = \nu, |\nu| < +\infty \tag{16}$$

where $E[A] = \underline{A}$, and ν is a gamma random variable.

$$\tilde{d}(A) = 2^{n(n-1)/4} \prod_{1 \leq i < j \leq n} dA_{ij} \tag{17}$$

Under the constraints of Equations (14)–(16), the MEP is used to construct the Lagrangian function to search for the optimal solution, and p_A can be calculated with

$$p_A(A) = c_A \times (\det A)^{\lambda-1} \times \exp\left(-\frac{n-1+2\lambda}{2} \text{tr}\left\{\underline{A}^{-1}A^T\right\}\right) \tag{18}$$

where c_A is a positive constant, which can be defined by

$$c_A = \frac{(2\pi)^{-n(n-1)/4} ((n+1)/2\delta^2)^{n(n-1+2\lambda)/2\delta^2}}{\left\{ \prod_{l=1}^n \Gamma((n+1)/2\delta^2 + (1-j)/2) \right\}} \tag{19}$$

where $\Gamma(x)$ represents the Gamma function; $tr(\cdot)$ represents the trace of the matrix; λ is the Lagrangian multiplier; and δ is the dispersion control parameter, and it can be calculated with the following formula.

$$\lambda = \frac{1}{2\delta^2} \left(1 - \delta^2(N-1) + \frac{(tr A)^2}{tr(A)^2} \right) \tag{20}$$

As can be seen from Equation (20), for a deterministic n , when λ approaches infinity, and δ approaches an infinitesimal value, A approaches \underline{A} by probability. In actual calculations, δ is an artificially given parameter, and thus, λ can be obtained through Equation (20).

3.2. Generation of Maximum Entropy Stochastic Models

This section will focus on how to generate A . The n -order matrix, A , is symmetric and positive, so the rank of matrix A is n , and it is convenient to use Cholesky decomposition in mathematical software. According to Reference [7], other decomposition methods will cause the two-factor matrix elements after decomposition to not have the properties of Equations (22) and (23). Therefore, Cholesky decomposition was chosen, and it can be calculated as follows:

$$A = L_A^T L_A \tag{21}$$

where the off-diagonal elements, $L_{n,ij}$ ($i < j$), of A are calculated with

$$L_{n,ij} = \sigma_n \mathbf{U}_{ij} \tag{22}$$

where $\sigma_n = \delta(n + 1)^{-1/2}$, and \mathbf{U}_{ij} obeys the standard Gaussian distribution. The diagonal elements of A are calculated with

$$L_{n,ii} = \sigma_n \sqrt{2v} \tag{23}$$

3.3. Construction of Nonparametric Riccati Whole Transfer Model

The Riccati whole mean transfer model is constructed in Sections 2.2 and 2.3; furthermore, the construction method of the maximum entropy random matrix is provided in Sections 3.1 and 3.2. Therefore, the nonparametric Riccati whole transfer model can be obtained by introducing a maximum entropy random matrix to the Riccati whole mean transfer model. At the same time, the following formula can be obtained using Equations (11) and (13):

$$B^T B = A^2 \tag{24}$$

The whole random transfer matrix, \mathbf{U}_{qr} ($q, r \in \{1,2\}$), does not have strict positive definiteness like the random matrix, B ; thus, \mathbf{U}_{qr} satisfies the following constraints from Equation (25):

$$(\mathbf{U}_{qr})^T \mathbf{U}_{qr} = A^2 \tag{25}$$

where \mathbf{U}_{qr} is the maximum entropy random matrix corresponding to the mean matrix, $\underline{\mathbf{U}}_{qr}$, in Equation (5). Similarly, the maximum entropy random matrices, $\mathbf{U}_{C,qr}$, at the coupling elements can be calculated as follows:

$$(\mathbf{U}_{C,qr})^T \mathbf{U}_{C,qr} = A^2 \tag{26}$$

From Equations (25) and (26), \mathbf{U}_{qr} and $\mathbf{U}_{C,qr}$ can be obtained and then substituted into Equations (5) and (9), respectively, to obtain the nonparametric Riccati whole transfer model of each element.

$$S_{i+1} = \left(\begin{bmatrix} \mathbf{u}_{11}^I & 0 \\ 0 & \mathbf{u}_{11}^{II} \end{bmatrix}_i S_i + \begin{bmatrix} \mathbf{u}_{12}^I & 0 \\ 0 & \mathbf{u}_{12}^{II} \end{bmatrix}_i \right) \cdot \left(\begin{bmatrix} \mathbf{u}_{21}^I & 0 \\ 0 & \mathbf{u}_{21}^{II} \end{bmatrix}_i S_i + \begin{bmatrix} \mathbf{u}_{22}^I & 0 \\ 0 & \mathbf{u}_{22}^{II} \end{bmatrix}_i \right)^{-1} \tag{27}$$

$$S_{C,i+1} = S_{C,i} + \begin{bmatrix} T_{C,12} & T_{C,14} \\ T_{C,32} & T_{C,34} \end{bmatrix}_i \tag{28}$$

From Equations (27) and (28), the nonparametric Riccati whole transfer matrix, $S_2 \dots S_{C,i} \dots S_{N+1}$, of each element in the system can be successively obtained. As such, a nonparametric Riccati whole transfer model of a dual-rotor system has been constructed successfully.

3.4. Solving the Critical Speeds and Vibration Modes

The start and end sections of the dual-rotor system shown in Figure 2 are both free ends, i.e., free boundary conditions.

$$[M^j, Q^j]_{N+1}^T = [M^j, Q^j]_1^T = [0 \ 0]^T \tag{29}$$

From the free boundary conditions and the nonparametric Riccati whole transfer matrices, $[S]_{N+1}$, the synchronous precession equation of the uncertain dual-rotor system can be obtained.

$$|S_{N+1}| = 0 \tag{30}$$

Although Equation (30) satisfies the above boundary conditions, the result includes not only the critical speeds of the system but also many singular points. These singular points are the zero points of the residual $\Delta(\omega)$ from negative infinity to positive infinity, not the critical speed points of the system. As a consequence, the following formula, which can eliminate these singular points, is used to calculate the critical speeds.

$$\Delta(\omega) = |S|_{N+1} \prod_{i=1}^N |[u_{21}S + u_{22}]_i| = 0 \tag{31}$$

The frequency scanning method is used to solve Equation (31), and the obtained roots are each order critical speeds of the system.

$$\{E\}_i = [U_{21}(S + R) + U_{22}]_i^{-1} \{E\}_{i+1} \tag{32}$$

The above formula is the recursive formula of the deformation state vector, where $\{E\}_i$ is the deformation state vector. $U_{21,i}$ and $U_{22,i}$ can be defined by

$$\begin{cases} U_{21,i} = \begin{bmatrix} U_{21}^I & 0 \\ 0 & U_{21}^{II} \end{bmatrix}_i \\ U_{22,i} = \begin{bmatrix} U_{22}^I & 0 \\ 0 & U_{22}^{II} \end{bmatrix}_i \end{cases} \tag{33}$$

According to the properties of Riccati transfer matrix, the proportional solution $\{E\}_i$ can be obtained. Let $\theta_{N+1}^{II} = 1$, the normalized state vector Z_{N+1} of the end section in the system can be obtained. From Equation (32), the state vectors of each element in the system can be obtained, thus each order vibration mode of the dual-rotor system can be obtained.

3.5. Calculation Process

As shown in Figure 3, the flow chart for calculating the dynamic characteristics of an uncertain dual-rotor system is provided. The specific steps are as follows: ① The structural parameters, material parameters, and operating parameters of the dual-rotor system are input. ② According to the structural characteristics of the system, the calculation model of the system is determined and the elements are divided. ③ A deterministic transfer model is constructed. ④ Through matrix transformation, the random asymmetric positive definite matrix, B , is decomposed into the product of a strict positive definite matrix, A , and a unitary matrix, D . ⑤ Based on MEP and RMT, a nonparametric transfer model is constructed. ⑥ A dynamic model with nonparametric uncertainty is obtained. ⑦ The natural characteristics of the system are calculated.

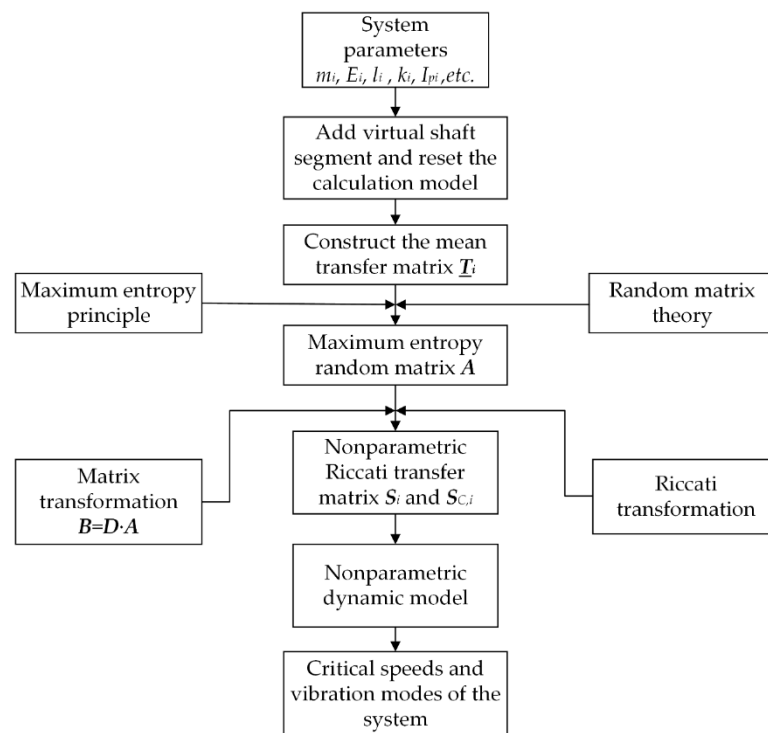


Figure 3. Flow chart for calculating the natural characteristics of the system.

4. Impacts of Two Uncertainties on Natural Characteristics

In this section, the nonparametric Riccati whole transfer model derived in Sections 2 and 3 is used to model the uncertain dual-rotor system shown in Figure 2. Through a great number of numerical simulations, under the same level of uncertainty, the effects of two types of uncertainties on the natural characteristics of the system are explored.

4.1. Impacts of Two Uncertainties at Intermediate Support Elements

In this section, the effects of parameter uncertainty and nonparametric uncertainty on the natural characteristics of the dual-rotor system are studied via numerical simulations. As shown in Figure 2, the ninth element is the intermediate support element connecting two rotors, and its uncertainties will greatly affect the whole transfer model. Therefore, the uncertainties at the intermediate support elements have to be analyzed under the same level of uncertainty so that one can compare the contribution of two types of uncertainties in the system. Due to the significant amount of calculation, only 100 numerical simulations utilizing the nonparametric model (NM) were finished. In comparison, 100 MCS were executed based on the parameter model (PM) proposed in Reference [29]. Furthermore, the results calculated via the mean model (MM) are provided.

In actual engineering applications, engineers often focus only on the low-order modes, because they have large amplitude, large equivalent mass, and are the most destructive. Therefore, only the first three-order modes of the system are analyzed in this paper.

Figure 4 shows the first three-order critical speeds of the system with a different $C_{ov,k}$. C_{ov} is the coefficient of variation, which is equivalent to δ in Equation (19). It is often set as 0.1 in practice [11]. In this paper, C_{ov} is set as 0–0.20 (0, 0.05, 0.10, 0.15, and 0.20) to study the impacts of two types of uncertainties on natural characteristics. In order to evaluate the impacts of uncertainties on the natural characteristics of the system, relative errors were introduced to characterize the changes in the first three-order critical speeds. It can be seen that the two types of uncertainties at the intermediary support element have similar impacts on the first three-order critical speeds from Table 2; that is, the relative errors of the critical speeds will increase with two uncertainties. At the same time, there are some differences. On the one hand, at the same level of uncertainty, the errors caused by nonparametric

uncertainty are significantly larger than those caused by parameter uncertainty, indicating that the first three-order critical speeds are more sensitive to nonparametric uncertainty. Capiez et al. [29] reached a similar conclusion when conducting a quantitative study on the uncertainty of complex aircraft. On the other hand, at the same level of uncertainty, the impacts will increase with the orders of critical speed, indicating that the high-order critical speeds are more sensitive to the parameter uncertainty than the low-order critical speeds. At the same level of nonparametric uncertainty, this rule cannot be established. The errors of n_{c2} are the smallest, followed by n_{c1} , and n_{c3} is the largest, which indicates that the impacts of nonparametric uncertainty on different-order critical speeds are different. In short, the critical speeds of the system will vary with its own orders and the type of uncertainty.

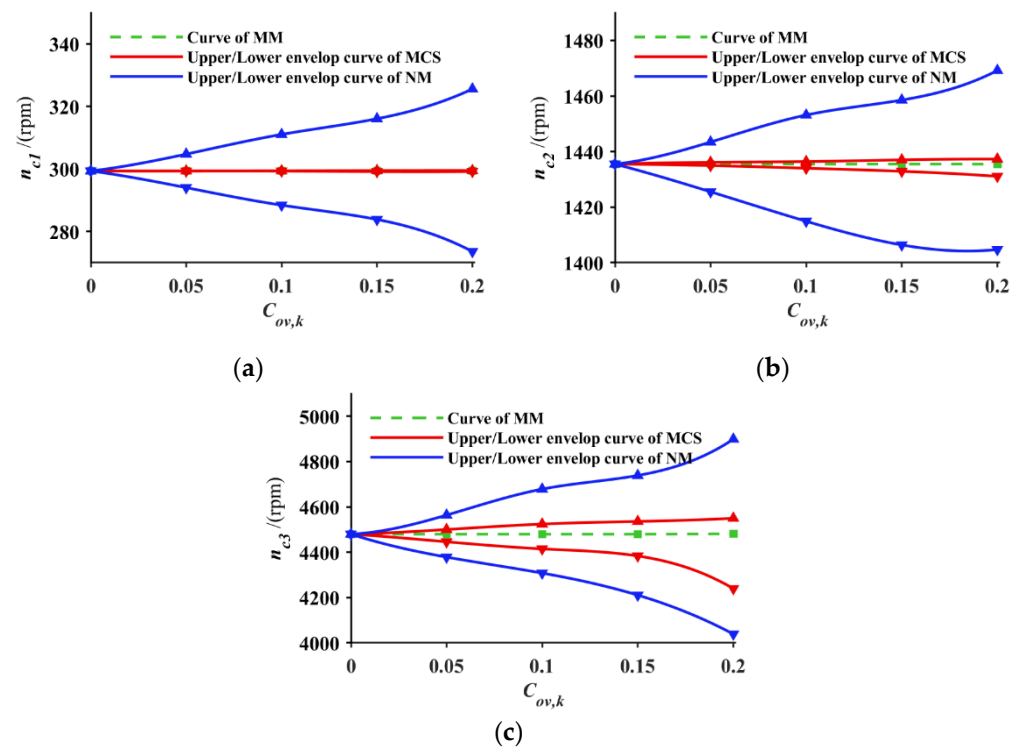


Figure 4. The first three-order critical speeds of the uncertain dual-rotor system for $C_{ov,k}$, from 0 to 0.20. (a) The first-order critical speed. (b) The second-order critical speed. (c) The third-order critical speed.

Table 2. Relative errors of the first three-order critical speeds of the system with two uncertainties at the intermediate support elements.

$C_{ov,k}$	Parameter Uncertainty			Nonparametric Uncertainty		
	n_{c1}	n_{c2}	n_{c3}	n_{c1}	n_{c2}	n_{c3}
0.05	0.010%	0.040%	0.591%	1.292%	0.624%	2.067%
0.10	0.014%	0.084%	1.154%	2.727%	1.331%	4.135%
0.15	0.037%	0.143%	1.589%	3.924%	1.816%	5.892%
0.20	0.035%	0.217%	3.343%	6.268%	2.245%	9.596%

The critical speeds reflect the speed range at which the rotor system resonates, but the vibration modes reflect the vibration form of the system, which is also an important natural characteristic of the rotor system. Therefore, it is necessary to analyze the uncertainty of the vibration modes. The modal assurance criteria (MAC) are used to analyze the effects

of two types of uncertainties on the first three-order vibration modes [30], which can be calculated as follows:

$$MAC = \frac{\left| [\varphi_a]^T [\varphi_b] \right|^2}{[\varphi_a]^T [\varphi_a] [\varphi_b]^T [\varphi_b]} \tag{34}$$

where $[\varphi_a]$ and $[\varphi_b]$ represent the vibration mode vectors obtained from the stochastic models (PM and NM) and the MM, respectively. From a mathematical point of view, the MAC represents the cosine value of two vectors in a specific space. The smaller the MAC value, the greater the angle between the two vectors, and it is easier to distinguish the two vectors. In the field of modal analysis, the smaller the MAC value is, the greater the difference between the vibration modes of the stochastic model and the MM, and the greater the impacts of uncertainties on the system’s natural characteristics. On the contrary, if the MAC value is closer to one, it means that the vibration modes of the stochastic model and MM are more similar, and the effects of uncertainty are lesser.

Figure 5 shows the upper and lower boundaries of the first three-order vibration modes of the system with two uncertainties for $C_{ov,k} = 0.20$. In order to show the floating degree of the rotor I and rotor II vibration modes more intuitively, the same order vibration modes of the two rotors were placed in one figure. The long lines represent the vibration modes of rotor I, and the short lines represent that of rotor II. The solid blue lines represent the vibration modes calculated with NM, the solid red lines represent those calculated with MCS, and the dotted green line represents those calculated with MM. These descriptions also apply to the following figures. The impacts of two uncertainties on the vibration modes can be easily observed in Figure 6. The MAC values obtained by MCS are almost identical to one, indicating that the parameter uncertainty has little impact on the first three-order vibration modes of two rotors, which means that the vibration modes are insensitive to parameter uncertainty. At the same time, the MAC values of the first three-order vibration modes of rotor I decreased significantly under nonparametric uncertainty, indicating that the vibration modes of rotor I are sensitive to nonparametric uncertainty.

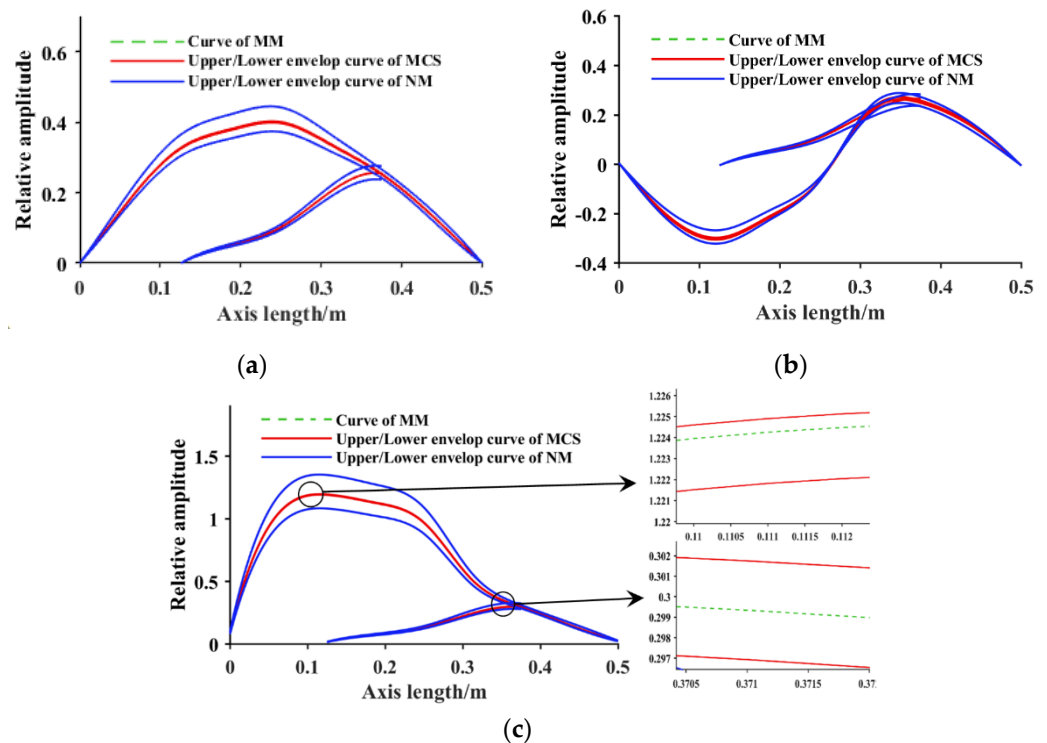


Figure 5. Upper and lower boundaries of the first three-order vibration modes of two rotors for $C_{ov,k} = 0.20$. (a) The first-order vibration mode. (b) The second-order vibration mode. (c) The third-order vibration mode.

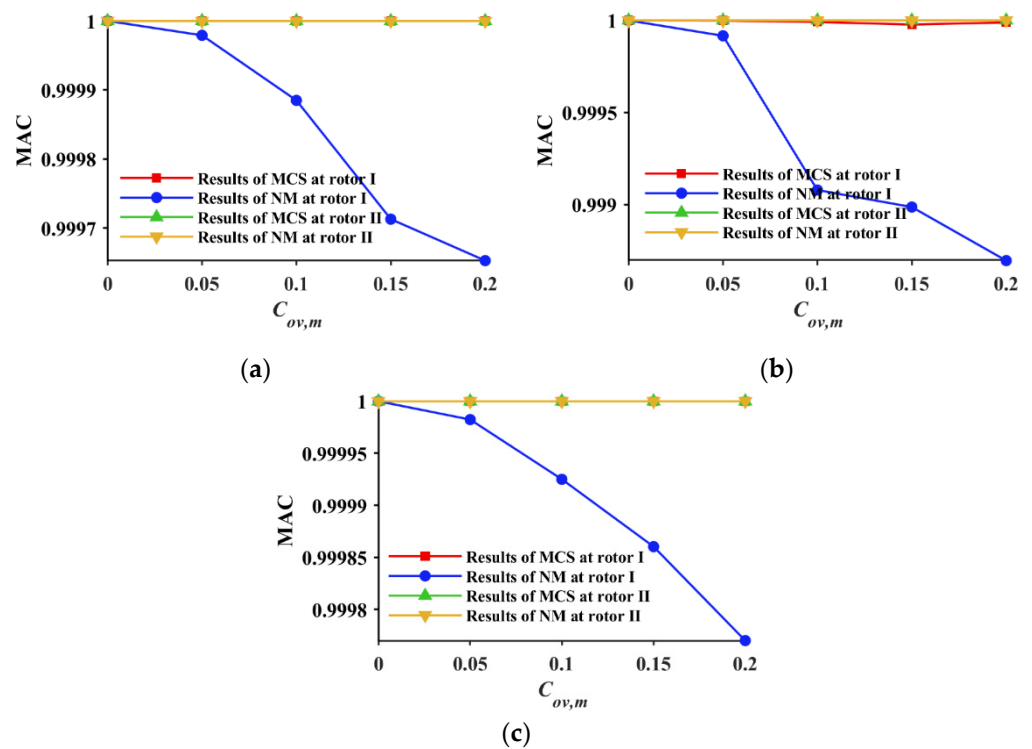


Figure 6. MAC values of the first three-order vibration modes of an uncertain dual-rotor system for $C_{ov,k} = 0-0.20$. (a) MAC values of the first-order vibration mode. (b) MAC values of the second-order vibration mode. (c) MAC values of the third-order vibration mode.

In short, the natural characteristics of the system are more sensitive to nonparametric uncertainty than to the parameter uncertainty at the intermediate supports.

4.2. Impacts of Two Uncertainties at Disk-Shaft Elements

In an actual dual-rotor system, the mass will also have a significantly large effect on the natural characteristics. In addition, it can be found from Equation (4) that the mass of elements is needed to construct the transfer matrices, so the mass parameter uncertainty will definitely affect the natural characteristics of the system. Therefore, this section will focus on the impacts of mass parameter uncertainty and nonparametric uncertainty at the 10th element on the natural characteristics of the dual-rotor system.

Figure 7 and Table 3 show the first three-order critical speeds of the system and their relative errors for $C_{ov,k} = 0-0.20$, respectively. For n_{c1} and n_{c2} , the results are similar to those in Section 4.1; i.e., the critical speeds of NM envelope those of PM. However, the results have changed for n_{c3} : the results of PM envelop those of NM, which indicates that the n_{c3} of this system is more sensitive to mass parameter uncertainty. Liu [20] drew a similar conclusion in studying the effects of uncertainties on the critical speeds of the rotating system.

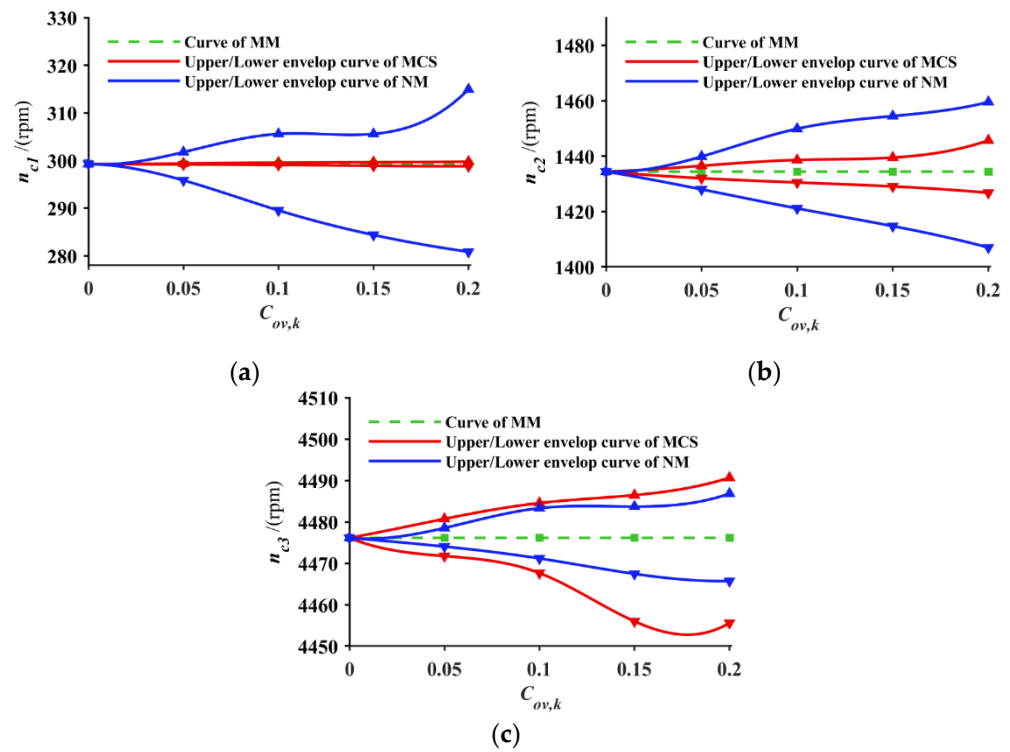


Figure 7. The first three-order critical speeds of the uncertain dual-rotor system for $C_{ov,m}$, from 0 to 0.20. (a) The first-order critical speed. (b) The second-order critical speed. (c) The third-order critical speed.

Table 3. Relative errors of the first three-order critical speeds of a system with two uncertainties at the disk-shaft element.

$C_{ov,m}$	Parameter Uncertainty			Nonparametric Uncertainty		
	n_{c1}	n_{c2}	n_{c3}	n_{c1}	n_{c2}	n_{c3}
0.05	0.048%	0.157%	0.050%	1.486%	0.413%	0.100%
0.10	0.096%	0.283%	0.135%	4.025%	1.002%	0.189%
0.15	0.168%	0.363%	0.181%	5.319%	1.385%	0.340%
0.20	0.240%	0.659%	0.236%	8.554%	1.831%	0.391%

As shown in Figure 8, under the impacts of mass parameter uncertainty and nonparametric uncertainty at the disk-shaft element, the first three-order vibration modes change; that is, they are no longer fixed in shape, instead constantly varying within a certain interval. It should be noted that both the second-order and third-order vibration modes display a phenomenon where the vibration modes under parameter uncertainty envelope those under nonparametric uncertainty, which is different from Figure 5, indicating that the mass uncertainty of the disk-shaft elements and the stiffness uncertainty of the intermediate supports have different impacts on the vibration modes. The MAC variation in Figure 9 also confirms the existence of this phenomenon. It may be due to the large mass of the 10th element, resulting in greater contributions from mass parameter uncertainty than the corresponding nonparametric uncertainty.

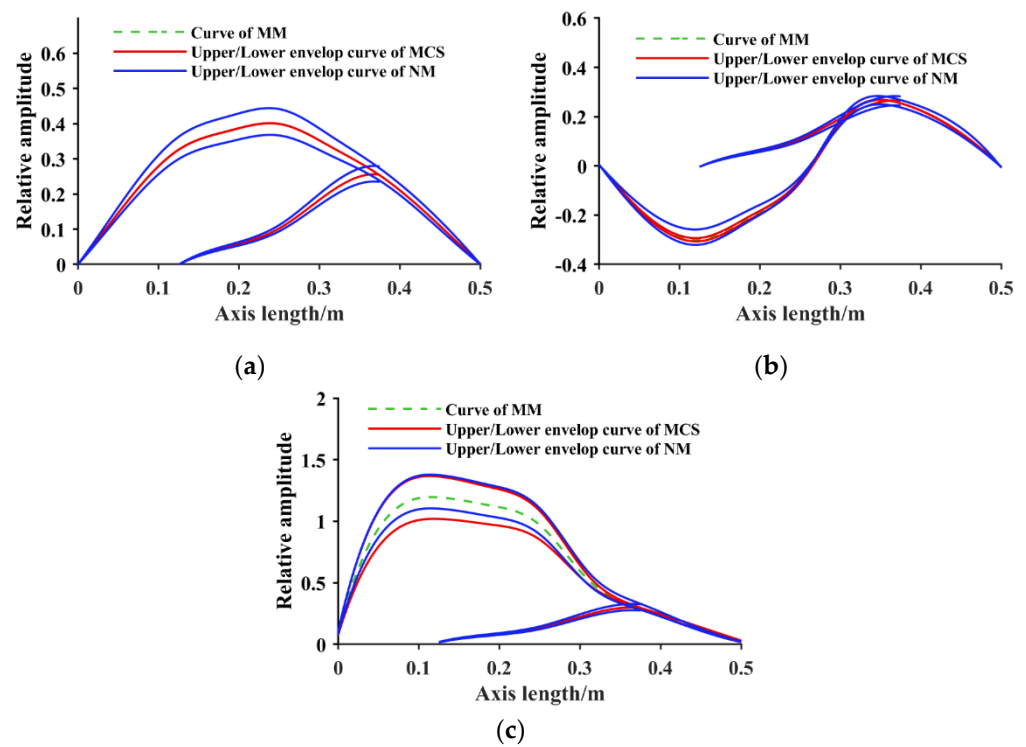


Figure 8. Upper and lower boundaries of the first three-order vibration modes of two rotors for $C_{ov,m} = 0.20$. (a) The first-order vibration mode. (b) The second-order vibration mode. (c) The third-order vibration mode.

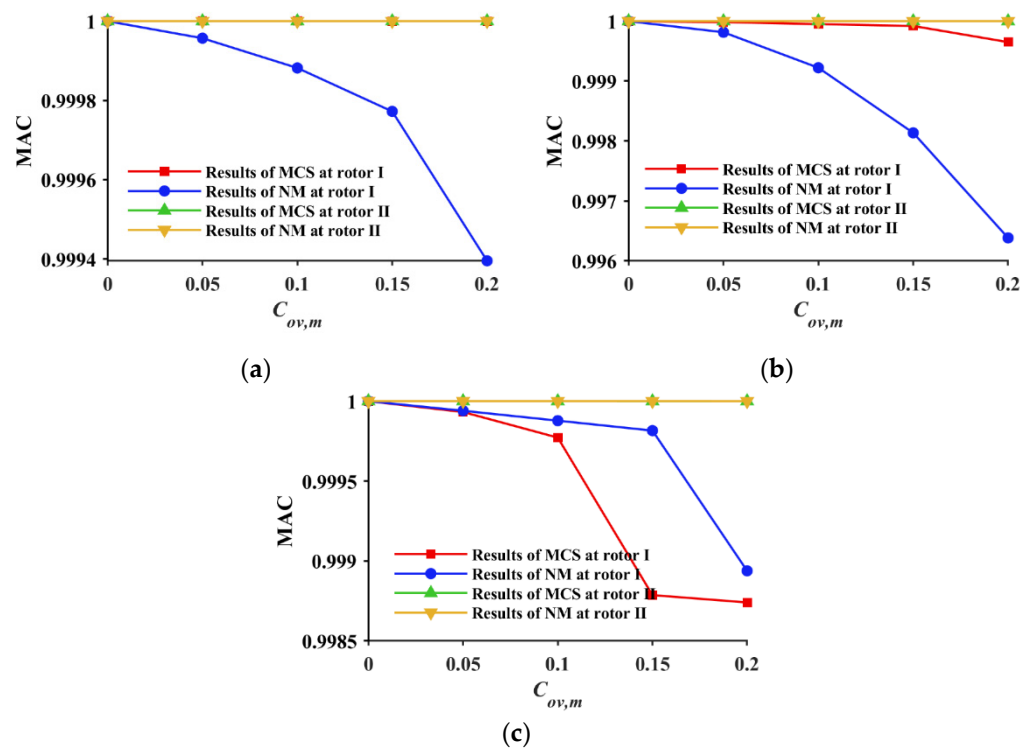


Figure 9. MAC values of the first three-order vibration modes of an uncertain dual-rotor system for $C_{ov,m} = 0-0.20$. (a) MAC values of the first-order vibration mode. (b) MAC values of the second-order vibration mode. (c) MAC values of the third-order vibration mode.

The above analyses reveal that the mass parameter uncertainty, stiffness parameter uncertainty, and the corresponding nonparametric uncertainty will alter the natural characteristics of the system. It can be concluded that, at the same level of uncertainty, the impacts of parameter uncertainty on the natural characteristics are smaller than that of nonparametric uncertainty in most cases. Moreover, the natural characteristics of the system will always strongly alter with the increase in uncertainties.

5. Conclusions

A nonparametric Riccati whole transfer model of an uncertain dual-rotor system is constructed based on Riccati transfer matrix theory, RMT, and MEP. Via matrix transformation, it is used to model an uncertain dual-rotor system or a multi-rotor system and to calculate the critical speeds and vibration modes of this system. Through multiple numerical simulations, the behavior of stiffness parameter uncertainty at the intermediate supports, mass parameter uncertainty at the disk-shaft elements, and the impact of corresponding nonparametric uncertainties on the natural characteristics of the system are analyzed respectively. The results show that both parameter uncertainty and nonparametric uncertainty will cause critical speeds to transform from deterministic values to interval values, and the vibration modes will also vary in intervals. In most cases, the natural characteristics are more sensitive to nonparametric uncertainty than to parameter uncertainty at the intermediate support elements and disk-shaft elements. However, the mass parameter uncertainty of the disk-shaft elements has a greater impact on the natural characteristics than the nonparametric uncertainty. This may be due to the large mass of the 10th element, thus reinforcing the role of mass parameter uncertainty. The results of this paper will be of great help to researchers in designing reliable dual-rotor and multi-rotor systems.

Author Contributions: H.W.: investigation, formal analysis, visualization, and writing—original draft. B.L.: review and supervision. Y.L.: software, review, and editing. W.F.: review and supervision. All authors have read and agreed to the published version of the manuscript.

Funding: This study received financial support from the National Natural Science Foundation of China (No. 12072106).

Conflicts of Interest: The authors declare that they have no known competing financial interest or personal relationships that could have appeared to influence the work reported in this paper.

References

1. Hong, J.; Wang, H.; Xiao, D.W.; Chen, M. Effects of dynamic stiffness of rotor bearing on rotor dynamic characteristics. *Aeroengine* **2008**, *1*, 23–27.
2. Nasir, F.E.; Fotuhi, M.J.; Bingul, Z. Linear and extended Kalman filter estimation of pitch and yaw angles for 2 DOF double dual twin rotor aerodynamical system. In Proceedings of the 2018 6th International Conference on Control Engineering & Information Technology (CEIT), Istanbul, Turkey, 25–27 October 2018.
3. Liu, Y.X.; Liu, B.G.; Feng, W.; Cheng, M. Vibration responses analysis for double disks rotor system with uncertainties. *J. Aerosp. Power* **2021**, *36*, 488–497.
4. Fu, C.; Sinou, J.J.; Zhu, W.D.; Lu, K.; Yang, Y.F. A state-of-the-art review on uncertainty analysis of rotor systems. *Mech. Syst. Signal Process.* **2023**, *183*, 109619. [[CrossRef](#)]
5. Chang, C.Y.; Chang, M.Y.; Huang, J.H. Vibration analysis of rotating composite shafts containing randomly oriented reinforcements. *Compos. Struct.* **2004**, *63*, 21–32. [[CrossRef](#)]
6. Der Kiureghian, A.; Ditlevsen, O. Aleatory or epistemic? Does it matter? *Struct. Saf.* **2009**, *31*, 105–112. [[CrossRef](#)]
7. Soize, C. *Uncertainty Quantification: An Accelerated Course with Advanced Applications in Computational Engineering*; Springer: Berlin/Heidelberg, Germany, 2017.
8. Feng, W.; Liu, B.G.; Ding, H.; Shen, H.P. Review of uncertain nonparametric dynamic modeling. *J. Vib. Shock* **2020**, *39*, 1–9.
9. Fu, C.; Feng, G.J.; Ma, J.J.; Lu, K.; Yang, Y.Y.; Gu, F.S. Predicting the dynamic response of dual-rotor system subject to interval parametric uncertainties based on the non-intrusive metamodel. *Mathematics* **2020**, *8*, 736. [[CrossRef](#)]
10. Fu, C.; Zhu, W.D.; Zheng, Z.L.; Sun, C.Z.; Yang, Y.Y.; Lu, K. Nonlinear responses of a dual-rotor system with rub-impact fault subject to interval uncertain parameters. *Mech. Syst. Signal Process.* **2022**, *170*, 108827. [[CrossRef](#)]
11. Wang, J.; Yang, Y.Y.; Zheng, Q.Y.; Deng, W.Q.; Zhang, D.S.; Fu, C. Dynamic Response of Dual-Disk Rotor System with Uncertainties Based on Chebyshev Convex Method. *Appl. Sci.* **2021**, *11*, 9146. [[CrossRef](#)]

12. Soize, C. A comprehensive overview of a nonparametric probabilistic approach of model uncertainties for predictive models in structural dynamics. *J. Sound Vib.* **2005**, *288*, 623–652. [[CrossRef](#)]
13. Soize, C. Maximum entropy approach for modeling random uncertainties in transient elastodynamics. *J. Acoust. Soc. Am.* **2001**, *109*, 1979–1996. [[CrossRef](#)] [[PubMed](#)]
14. Soize, C. Random matrix theory and nonparametric model of random uncertainties in vibration analysis. *J. Sound Vib.* **2003**, *263*, 893–916. [[CrossRef](#)]
15. Soize, C. Random matrix theory for modeling uncertainties in computational mechanics. *Comput. Methods Appl. Mech. Eng.* **2005**, *194*, 1333–1366. [[CrossRef](#)]
16. Murthy, R.; Mignolet, M.P.; El-Shafei, A. Nonparametric stochastic modeling of uncertainty in rotordynamics-part II: Applications. *J. Eng. Gas Turbines Power* **2010**, *132*. [[CrossRef](#)]
17. Gan, C.B.; Wang, Y.H.; Yang, S.X. Nonparametric modeling on random uncertainty and reliability analysis of a dual-span rotor. *J. Zhejiang Univ. Sci. A* **2018**, *19*, 189–202. [[CrossRef](#)]
18. GANCB; Wang, Y.H.; Yang, S.X.; Cao, Y.L. Nonparametric modeling and vibration analysis of uncertain Jeffcott rotor with disc offset. *Int. J. Mech. Sci.* **2014**, *78*, 126–134.
19. Huang, W.D.; Gan, C.B. Bifurcation analysis and vibration signal identification for a motorized spindle with random uncertainty. *Int. J. Bifurc. Chaos* **2019**, *29*, 1951–1967. [[CrossRef](#)]
20. Liu, Y.X.; Liu, B.G.; Cheng, M.; Feng, W. Natural frequency analysis of a dual-rotor system with model uncertainty. *Arch. Appl. Mech.* **2022**, *92*, 2495–2508. [[CrossRef](#)]
21. Chai, S.; Gang, X.; Qu, Q. A whole transfer matrix method for the eigensolutions of multi-rotor systems. *ASME Power Conf.* **2005**, *41820*, 457–463.
22. Jiang, S.Y.; Lin, S.Y. Study on dynamic characteristics of motorized spindle rotor-bearing-housing system. *J. Mech. Eng.* **2021**, *57*, 1–10.
23. Tuan, L.A.; Cuong, H.M.; Lee, S.G.; Nho, L.C.; Moon, K. Nonlinear feedback control of container crane mounted on elastic foundation with the flexibility of suspended cable. *J. Vib. Control* **2016**, *22*, 3067–3078. [[CrossRef](#)]
24. Masoud, Z.N. Effect of hoisting cable elasticity on anti-sway controllers of quay-side container cranes. *Nonlinear Dyn.* **2009**, *58*, 129–140. [[CrossRef](#)]
25. Arena, A.; Casalotti, A.; Lacarbonara, W. Three-dimensional modeling of container cranes. In Proceedings of the International Design Engineering. In Proceedings of the Technical Conferences and Computers and Information in Engineering Conference, Portland, OR, USA, 4–7 August 2013; Volume 55966, p. V07AT10A069.
26. Soize, C. Stochastic modeling of uncertainties in computational structural dynamics-recent theoretical advances. *J. Sound Vib.* **2013**, *332*, 2379–2395. [[CrossRef](#)]
27. Vance, J.M.; Zeidan, F.Y.; Murphy, B.G. *Machinery Vibration and Rotordynamics*; John Wiley & Sons: Hoboken, NJ, USA, 2010.
28. Wishart, J. The generalized product moment distribution in samples from a normal multivariate population. *Biometrika* **1928**, *20A*, 32–52. [[CrossRef](#)]
29. Capiez-Lernout, E.; Soize, C. Nonparametric modeling of random uncertainties for dynamic response of mistuned bladed disks. *J. Eng. Gas Turbines Power* **2004**, *126*, 610–618. [[CrossRef](#)]
30. Yang, Y.; Tan, X.K.; Wang, H.; Wang, R.Q.; Tian, K. Research on a new method of beam bridge mode shape identification based on statistical moment theory. *China J. Highw. Transp.* **2022**, 1–16.